Remaining Opportunities in Capacitive Power Transfer Based on Duality with Inductive Power Transfer

Yao Wang, *Student Member, IEEE*, Hua Zhang, *Member, IEEE*, Yue Cao, *Senior Member, IEEE*, Fei Lu, *Member, IEEE*

***Abstract*—Wireless power transfer (WPT) has proven to be an effective solution for electric vehicle charging. As two mainstream near-field WPT technologies, inductive and capacitive power transfer (IPT and CPT) have many similarities. This paper aims to explore the remaining opportunities in CPT systems, not yet reported in existing literature, based on duality with the mature IPT technology. First, a generic modeling method based on two-port network theory is proposed, which contributes to unified modeling and analysis for both inductive and capacitive couplings. Then, power transfer mechanism of IPT and CPT couplers is compared, and unified transfer efficiency is derived, promoting CPT theory developments. Last, the duality between existing IPT and CPT circuits is demonstrated in two aspects: compensation circuit configuration and resonant relationship. 14 CPT topologies are derived based on duality with the existing 7 mainstream IPT circuits, of which 11 circuits do not exist in literature, offering future opportunities in CPT. Detailed comparison and evaluation of the derived 14 CPT circuits are conducted, and high-performance circuits are recommended. As a demonstration, a case study of a 2.1kW 3MHz CPT system is implemented in hardware based on the newly proposed M_1-*SS* topology. This example system achieves a peak efficiency of 93.19% with the predicted circuit properties of load-independent constant-voltage (CV) output and zero-phase-angle (ZPA) property.**

***Index Terms*—Capacitive power transfer, inductive power transfer, duality, two-port parameter.**

I. Introduction

Wireless power transfer (WPT) technology has shown great potential in electric vehicle (EV) charging [1]-[3], which gets rid of troublesome cables and can utilize underground installation, allowing higher space utilization, convenience, and safety over conventional conductive charging [4]-[6].

Inductive power transfer (IPT) and capacitive power transfer (CPT) are two mainstream WPT technologies for EV charging [7]-[9]. In principle, IPT achieves power transfer via an alternating magnetic field generated by a pair of mutually coupled coils while CPT relies on an alternating electric field of two pairs of metal plates, shown in Figs. 1 and 2, respectively. IPT and CPT distinguish each other in couplers and fields. Meantime, similarities are also identifiable [10], typically in the compensation circuit designs. For example, in an IPT system, there are four basic two-capacitor compensation circuits, namely, series-series (SS), series-parallel (SP), parallel-series (PS), and parallel-parallel (PP) [11]-[14]. Likewise, four basic two-inductor compensations have also been proposed for a CPT coupler with same configurations [15]-[18]. In another description, CPT technology could be considered as a reflection of IPT in a special "mirror". Such a property is named duality between IPT and CPT systems in this paper.

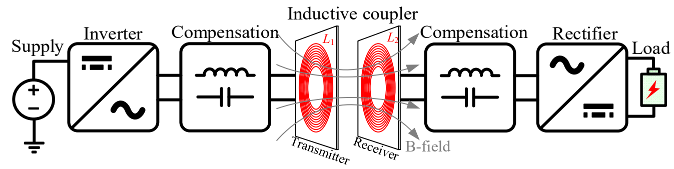

Fig.1 Structure of an inductive power transfer system.

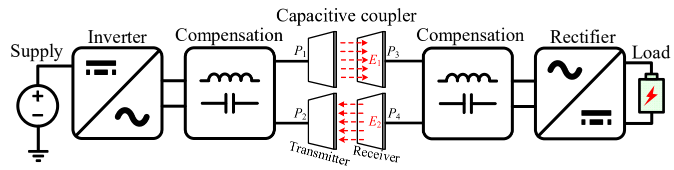

Fig.2 Structure of a capacitive power transfer system.

IPT has been developed for over 100 years and achieved success in EVs, medical equipment, and consumer electronics [19]-[21]. However, the bulky and expensive IPT coupler and the eddy current loss limit practical applications [22]-[23]. CPT is proposed within 20 years [24] with advantages of light weight, no eddy current loss, and good misalignment tolerance, which can be applied where the IPT is not convenient, such as in underwater applications and metal-intensive motor scenarios [22], [23]. However, due to a short history, the basic theory research and circuit opportunities of CPT technology are still insufficient. Besides, the existing research that explores feasible CPT circuits [17]-[18], [25]-[28] is limited to one particular topology, lacking systematic discovery and analysis of all applicable high-performance CPT circuits. This paper hence presents a methodology to comprehensively explore remaining CPT opportunities that are not yet reported in literature based on the duality between CPT and mature IPT technologies.

The paper's main contributions are summarized as follows. First, a generic modeling method based on the two-port network theory is proposed, which contributes to a standardized and unified modeling method for both IPT and CPT systems. Second, the power transfer mechanism of IPT and CPT systems is compared in detail, and unified transfer efficiency is derived for both couplers, revealing their similarity and promoting the CPT theory development. Third, the duality between IPT and CPT circuits is demonstrated in terms of the compensation circuit configuration and resonant relationship.

Manuscript received July 25, 2022; revised Oct. 24, 2022, accepted Nov. 27, 2022. This work was supported by the Advanced Research Projects Agency-Energy, U.S. Department of Energy under Grant DE-AR0001114 in the BREAKERS program. *(Corresponding Author: Fei Lu)*

Yao Wang, and Fei Lu are with the Department of Electrical and Computer Engineering, Drexel University, Philadelphia, PA 19104, USA. (e-mail: yw696@drexel.edu; fei.lu@drexel.edu).

Hua Zhang is with the Department of Electrical Engineering, Rowan University, Glassboro, NJ 08028 USA (e-mail: hua.zhang@drexel.edu).

Yue Cao is with the Department of Electrical and Computer Engineering, Oregon State University, Corvallis, OR 97331 USA (e-mail: yue.cao@oregonstate.edu)

This article has been accepted for publication in IEEE Transactions on Transportation Electrification. This is the author's version which has not been fully edited and content may change prior to final publication. Citation information: DOI 10.1109/TTE.2022.3225578

Table I Description of IPT and CPT couplers.

Property	Inductive coupler	Capacitive coupler
Structure	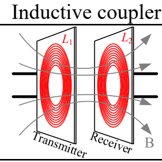	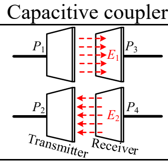
Coupling	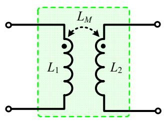	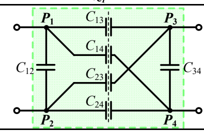
Self-*L*/*C*	L_1, L_2	C_1, C_2
Mutual coupling	L_M	C_M
Coupling coeff.	$k_L=L_M/(L_1L_2)^{0.5}$	$k_C=C_M/(C_1C_2)^{0.5}$

14 CPT topologies can be derived in duality with existing 7 mainstream IPT circuits, of which 11 CPT circuits are not yet reported in the existing literature. Furthermore, detailed comparison and evaluation of the derived 14 CPT circuits are conducted, and high-performance circuits are recommended. One case study of a 2.1kW 3MHz M_1-*SS* CPT system is constructed in hardware, validating the demonstrated duality investigation.

II. Modeling of Inductive and Capacitive Couplings

A. Standardized Definition of IPT and CPT Couplers

The inductive coupler consists of two coils L_1 and L_2, and the mutually coupled magnetic field transfers power, as shown in Fig.1. An inductive coupler is generally described by self-inductances L_1 and L_2, and mutual inductance L_M (or coupling coefficient k_L).

A typical capacitive coupler includes four metal plates, P_1~P_4, as shown in Fig.2. The electric field between the plates contributes to power transfer. The six-capacitor modeling can be used to demonstrate the capacitive couplings in a four-plate CPT coupler, shown in Table I. C_{13} and C_{24} are the main couplings between plate pairs P_1 and P_3, P_2 and P_4; C_{14} and C_{23} are cross-couplings between P_1 and P_4, P_2 and P_3; C_{12} and C_{34} are shunt capacitances between P_1 and P_2, P_3 and P_4. According to [28], self-capacitance C_1, C_2, and mutual capacitance C_M can be defined in (1).

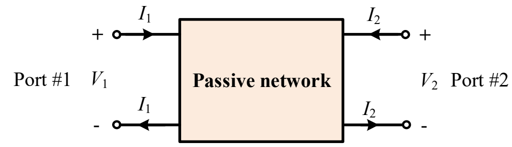

Fig.3 A typical two-port network.

Table II Description of four two-port parameters [29].

Parameters	Description	Calculation
z-parameter	$\begin{cases} V_1 = z_{11}I_1 + z_{12}I_2 \\ V_2 = z_{21}I_1 + z_{22}I_2 \end{cases}$	$\begin{cases} z_{11} = \frac{V_1}{I_1}\Big\vert_{I_2=0}, \ z_{12} = \frac{V_1}{I_2}\Big\vert_{I_1=0} \\ z_{21} = \frac{V_2}{I_1}\Big\vert_{I_2=0}, \ z_{22} = \frac{V_2}{I_2}\Big\vert_{I_1=0} \end{cases}$
y-parameter	$\begin{cases} I_1 = y_{11}V_1 + y_{12}V_2 \\ I_2 = y_{21}V_1 + y_{22}V_2 \end{cases}$	$\begin{cases} y_{11} = \frac{I_1}{V_1}\Big\vert_{V_2=0}, \ y_{12} = \frac{I_1}{V_2}\Big\vert_{V_1=0} \\ y_{21} = \frac{I_2}{V_1}\Big\vert_{V_2=0}, \ y_{22} = \frac{I_2}{V_2}\Big\vert_{V_1=0} \end{cases}$
h-parameter	$\begin{cases} V_1 = h_{11}I_1 + h_{12}V_2 \\ I_2 = h_{21}I_1 + h_{22}V_2 \end{cases}$	$\begin{cases} h_{11} = \frac{V_1}{I_1}\Big\vert_{V_2=0}, \ h_{12} = \frac{V_1}{V_2}\Big\vert_{I_1=0} \\ h_{21} = \frac{I_2}{I_1}\Big\vert_{V_2=0}, \ h_{22} = \frac{I_2}{V_2}\Big\vert_{I_1=0} \end{cases}$
g-parameter	$\begin{cases} I_1 = g_{11}V_1 + g_{12}I_2 \\ V_2 = g_{21}V_1 + g_{22}I_2 \end{cases}$	$\begin{cases} g_{11} = \frac{I_1}{V_1}\Big\vert_{I_2=0}, \ g_{12} = \frac{I_1}{I_2}\Big\vert_{V_1=0} \\ g_{21} = \frac{V_2}{V_1}\Big\vert_{I_2=0}, \ g_{22} = \frac{V_2}{I_2}\Big\vert_{V_1=0} \end{cases}$

Table III. Behavior-source models of inductive coupler.

z-parameters	*y*-parameters	*h*-parameters	*g*-parameters
$\begin{cases} V_1 = I_1 j\omega L_1 + I_2 j\omega L_M \\ V_2 = I_1 j\omega L_M + I_2 j\omega L_2 \end{cases}$	$\begin{cases} I_1 = \frac{V_1}{j\omega L_1(1-k_L^2)} - \frac{V_2}{j\omega L_M(1/k_L^2-1)} \\ I_2 = -\frac{V_1}{j\omega L_M(1/k_L^2-1)} + \frac{V_2}{j\omega L_2(1-k_L^2)} \end{cases}$	$\begin{cases} V_1 = I_1 j\omega L_1(1-k_L^2) + V_2\frac{L_M}{L_2} \\ I_2 = -I_1\frac{L_M}{L_2} + V_2\frac{1}{j\omega L_2} \end{cases}$	$\begin{cases} I_1 = V_1\frac{1}{j\omega L_1} - I_2\frac{L_M}{L_1} \\ V_2 = V_1\frac{L_M}{L_1} + I_2 j\omega L_2(1-k_L^2) \end{cases}$
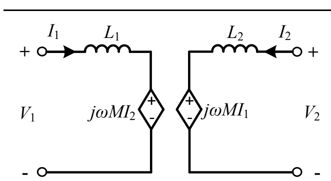	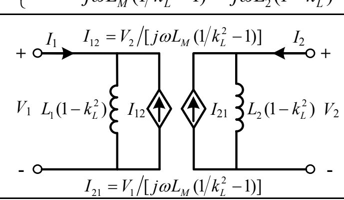	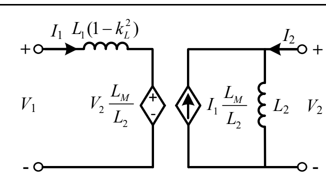	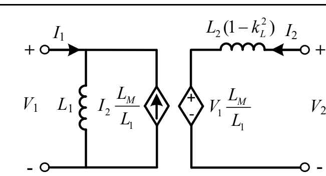

Table IV. Behavior-source models of capacitive coupler [29].

z-parameters	*y*-parameters	*h*-parameters	*g*-parameters
$\begin{cases} V_1 = \frac{I_1}{j\omega C_1(1-k_C^2)} + \frac{I_2}{j\omega C_M(1/k_C^2-1)} \\ V_2 = \frac{I_1}{j\omega C_M(1/k_C^2-1)} + \frac{I_2}{j\omega C_2(1-k_C^2)} \end{cases}$	$\begin{cases} I_1 = j\omega C_1V_1 - j\omega C_MV_2 \\ I_2 = -j\omega C_MV_1 + j\omega C_2V_2 \end{cases}$	$\begin{cases} V_1 = \frac{I_1}{j\omega C_1} + V_2\cdot\frac{C_M}{C_1} \\ I_2 = -I_1\cdot\frac{C_M}{C_1} + V_2\cdot j\omega C_2(1-k_C^2) \end{cases}$	$\begin{cases} I_1 = V_1\cdot j\omega C_1(1-k_C^2) - I_2\cdot\frac{C_M}{C_2} \\ V_2 = V_1\cdot\frac{C_M}{C_2} + \frac{I_2}{j\omega C_2} \end{cases}$
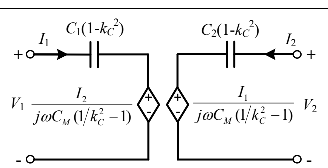	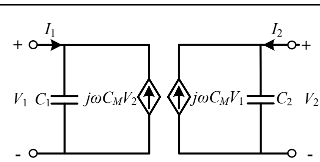	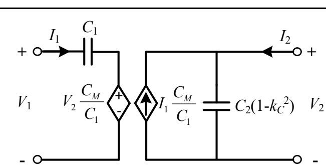	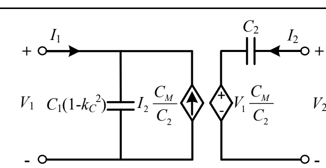

$$\begin{cases} C_1 = C_{12} + \dfrac{(C_{13}+C_{14})\cdot(C_{23}+C_{24})}{C_{13}+C_{14}+C_{23}+C_{24}} \\ C_2 = C_{34} + \dfrac{(C_{13}+C_{23})\cdot(C_{14}+C_{24})}{C_{13}+C_{14}+C_{23}+C_{24}} \\ C_M = \dfrac{C_{13}\cdot C_{24} - C_{23}\cdot C_{14}}{C_{13}+C_{14}+C_{23}+C_{24}} \end{cases} \quad (1)$$

Table I summarizes these concepts and notations, achieving similar descriptions for IPT and CPT couplers.

B. Generic Two-Port Parameter Modeling

Both IPT and CPT couplers can be considered a two-port circuit network. Each port consists of two terminals and satisfies the port condition: the current flowing into one terminal must equal the current flowing out of the other, which is demonstrated in Fig. 3. Considering this, a generic modeling method is proposed based on two-port network theory.

In Fig. 3, a two-port network includes 4 variables: V_1, I_1, V_2, and I_2. Each port has an independent excitation, either voltage or current. According to the two-port network theory [29], there exist four categories of parameters, namely: *z*-parameters (impedance), *y*-parameters (admittance), *h*-parameters (hybrid), and *g*-parameters (inverse hybrid), as described in Table II.

In each two-port parameter model, the network is linearly described by two independent excitations and four coefficients. It helps derive the equivalent behavior-source models of IPT and CPT coupler, respectively provided in Tables III and IV. For example, the inductive or capacitive coupler is equivalent to a behavior-voltage-source circuit by *z*-parameters, or a behavior-current-source circuit by *y*-parameters. Particularly, the two-port modeling for capacitive coupling has been reported in [29] while its application in IPT systems has not been clearly discussed.

C. Power Transfer Mechanism

The description of the power transfer mechanism of inductive and capacitive couplers is provided in Table V. In both IPT and CPT couplers, the power flow from primary to secondary side is represented by S_{12}, including both the active power P_{12} and the reactive power Q_{12} [19], [29].

1) Inductive Power Transfer

As shown in Table V, for an inductive coupler, the inductive coupling is equivalent to two behavior-voltage-sources V_{12} and V_{21} based on *z*-parameter modeling. Current $\boldsymbol{I}_2$ is taken as the reference phasor and the phase angle of $\boldsymbol{I}_1$ is represented by θ_{12}. Then, $\boldsymbol{I}_2$ is expressed below.

$$\boldsymbol{I}_1 = |I_1|(\cos\theta_{12} + j\sin\theta_{12}) \quad (2)$$

In an IPT coupler, the power flow S_{12} is calculated:

$$\boldsymbol{S}_{12}|_{IPT} = \boldsymbol{V}_{12}\cdot\boldsymbol{I}_1^* = \omega L_M I_1 I_2 \sin\theta_{12} + j\omega L_M I_1 I_2 \cos\theta_{12} \quad (3)$$

P_{12} and Q_{12} in an inductive coupler are provided below:

$$\begin{cases} P_{12}|_{IPT} = \mathrm{Re}[\boldsymbol{S}_{12}|_{IPT}] = \omega L_M I_1 I_2 \sin\theta_{12} \\ Q_{12}|_{IPT} = \mathrm{Im}[\boldsymbol{S}_{12}|_{IPT}] = \omega L_M I_1 I_2 \cos\theta_{12} \end{cases} \quad (4)$$

In an IPT coupler, P_{12} and Q_{12} are jointly determined by ω, L_M, I_1, I_2 and θ_{12}. P_{12} should be maximized to achieve effective power transfer while Q_{12} should be suppressed to reduce the Volt-Ampere (VA) rating and power loss. Namely, phase angle θ_{12} should be as close to 90° as possible, which can be

Table V. Power transfer mechanism of IPT and CPT coupler.

Inductive coupler	Capacitive coupler
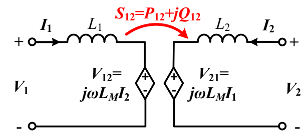	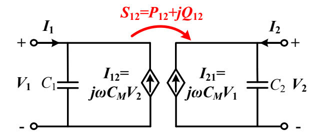
Power flow	Power flow
$\boldsymbol{S}_{12} = \boldsymbol{V}_{12}\cdot\boldsymbol{I}_1^* = P_{12} + jQ_{12}$	$\boldsymbol{S}_{12} = \boldsymbol{V}_1\cdot(-\boldsymbol{I}_{12}^*) = P_{12} + jQ_{12}$
Reference phasor	Reference phasor
$\boldsymbol{I}_2 = I_2\angle 0°,\ \boldsymbol{I}_1 = I_1\angle\theta_{12}$	$\boldsymbol{V}_1 = V_1\angle 0°,\ \boldsymbol{V}_2 = V_2\angle\varphi_{21}$

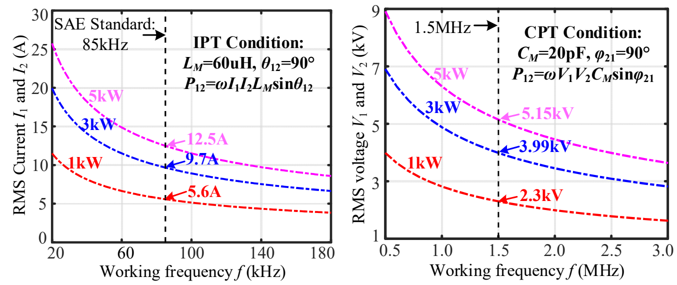

Fig.4 (a) IPT coil currents I_1 and I_2 *vs*. frequency *f* at specific power level; (b) CPT port voltage V_1 and V_2 *vs*. frequency *f* at specific power level. (I_1 and I_2, V_1 and V_2 are assumed to be the same, respectively.)

achieved by double-sided compensation capacitors.

In an IPT system, with a specified power level P_{12} and assuming identical current stress on primary and secondary coils, the coil currents I_1 and I_2 can be calculated by:

$$I_1 = I_2 = \sqrt{\frac{P_{12}}{\omega L_M \sin\theta_{12}}} \quad (5)$$

In practice, it is easy for an IPT coupler to achieve a mutual inductance L_M of tens of microhenry (μH). For example, with L_M=60μH and θ_{12}=90°, the coil currents versus working frequency under a given power are provided in Fig. 4 (a). It shows that the IPT system can easily achieve several kW at 85kHz and tens of amperes.

2) Capacitive Power Transfer

As shown in Table V, for a capacitive coupler, behavior-current sources I_{12} and I_{21} are introduced based on the *y*-parameters. Voltage $\boldsymbol{V}_1$ is considered as the reference phasor and the phase angle of $\boldsymbol{V}_2$ is represented by φ_{21}, namely:

$$\boldsymbol{V}_2 = |V_2|(\cos\varphi_{21} + j\sin\varphi_{21}) \quad (6)$$

Then, in a CPT coupler, the power flow S_{12} is calculated as:

$$\boldsymbol{S}_{12}|_{CPT} = \boldsymbol{V}_1\cdot(-\boldsymbol{I}_{12}^*) = \omega C_M V_1 V_2 \sin\varphi_{21} + j\omega C_M V_1 V_2 \cos\varphi_{21} \quad (7)$$

P_{12} and Q_{12} in a capacitive coupler are provided as:

$$\begin{cases} P_{12}|_{CPT} = \mathrm{Re}[\boldsymbol{S}_{12}|_{CPT}] = \omega C_M V_1 V_2 \sin\varphi_{21} \\ Q_{12}|_{CPT} = \mathrm{Im}[\boldsymbol{S}_{12}|_{CPT}] = \omega C_M V_1 V_2 \cos\varphi_{21} \end{cases} \quad (8)$$

In a CPT coupler, P_{12} and Q_{12} are determined by ω, C_M, V_1, V_2, and φ_{21}. Similar to an IPT coupler, to maximize P_{12} and minimize Q_{12}, φ_{21} should be close to 90°, which can be achieved by using double-sided compensation inductors.

In a CPT system, with specified power level P_{12} and identical port voltages of V_1=V_2, V_1 and V_2 can be calculated by:

$$V_1 = V_2 = \sqrt{\frac{P_{12}}{\omega C_M \sin\varphi_{21}}} \quad (9)$$

The capacitive coupling is usually much weaker than the

This article has been accepted for publication in IEEE Transactions on Transportation Electrification. This is the author's version which has not been fully edited and content may change prior to final publication. Citation information: DOI 10.1109/TTE.2022.3225578

magnetic coupling. Typically, the coupling capacitance C_M in an air-based CPT coupler is only at the picofarad (pF) level. To reach an effective power transfer of kilowatts, the frequency f and voltages V_1 and V_2 generally need to achieve megahertz (MHz) and kilovolt (kV) levels, as shown in Fig.4 (b). For example, with C_M=20pF and f=1.5MHz, the voltages V_1 and V_2 must achieve 3.99kV to enable a 3kW power transfer.

Furthermore, in an IPT system, the voltages across the transmitter and receiver plates are respectively defined as V_{CM1} and V_{CM2}, which can be calculated by:

$$V_{CM1}=V_{CM2}=\frac{|V_1-V_2|}{2}=\frac{\sqrt{V_1^2+V_2^2-2V_1V_2\cos\varphi_{21}}}{2} \quad (10)$$

Particularly, when V_1=V_2 is achieved, with specified P_{12}, ω, and C_M, voltages V_{CM1} and V_{CM2} are provided below.

$$V_{CM1}=V_{CM2}=\sqrt{\frac{V_1V_2(1-\cos\varphi_{21})}{2}}=\sqrt{\frac{P_{12}}{2\omega C_M}\cdot\tan\frac{\varphi_{21}}{2}} \quad (11)$$

D. Transfer Efficiency of IPT and CPT Couplers

In a real IPT or CPT system, the parasitic resistances of the coupler will cause power loss. Considering parasitic resistances, the IPT and CPT systems are modeled as Figs. 5 and 6. For an IPT coupler, R_{L1} and R_{L2} are series-modeled with L_1 and L_2 while in a CPT coupler, R_{C1} and R_{C2} are parallel-modeled with C_1 and C_2. In addition, the equivalent load resistance is defined as R_{Le}.

1) Transfer Efficiency of IPT Coupler

For an IPT coupler, the quality factors of inductors L_1 and L_2 are represented by Q_{L1} and Q_{L2}, defined as:

$$Q_{L1}=\omega L_1/R_{L1},\ \ Q_{L2}=\omega L_2/R_{L2} \quad (12)$$

Then, the transfer efficiency of an inductive coupler is calculated as:

$$\eta_{IPT}=\frac{I_2^2R_{Le}}{I_1^2R_{L1}+I_2^2R_{L2}+I_2^2R_{Le}}=\frac{1}{\frac{(R_{Le}+R_{L2})^2}{k_L^2Q_{L1}Q_{L2}R_{L2}R_{Le}}+\frac{R_{L2}}{R_{Le}}+1} \quad (13)$$

With a_L=R_{Le}/R_{L2}, (13) is simplified:

$$\eta_{IPT}=\frac{1}{1+\frac{1}{a_L}+\frac{1}{k_L^2Q_{L1}Q_{L2}}(a_L+\frac{1}{a_L}+2)} \quad (14)$$

2) Transfer Efficiency of CPT Coupler

For a CPT coupler, the quality factors are defined as:

$$Q_{C1}=\omega C_1R_{C1},\ \ Q_{C2}=\omega C_1R_{C2} \quad (15)$$

The transfer efficiency of a capacitive coupler is calculated:

$$\eta_{CPT}=\frac{V_2^2/R_{Le}}{V_1^2/R_{C1}+V_2^2/R_{C2}+V_2^2/R_{Le}}=\frac{1}{\frac{(R_{Le}+R_{C2})^2}{k_C^2Q_{C1}Q_{C2}R_{C2}R_{Le}}+\frac{R_{Le}}{R_{C2}}+1} \quad (16)$$

With a_C=R_{C2}/R_{Le}, (16) is simplified as:

$$\eta_{CPT}=\frac{1}{1+\frac{1}{a_C}+\frac{1}{k_C^2Q_{C1}Q_{C2}}(a_C+\frac{1}{a_C}+2)} \quad (17)$$

From (14) and (17), the inductive and capacitive couplers have a unified expression of transfer efficiency, which is mainly determined by coupling coefficient, quality factors, and load condition. Furthermore, it is also noted that (14) and (17) are not limited to calculating the transfer efficiency of

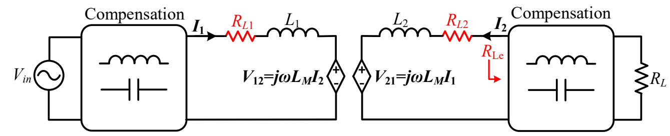

Fig.5. Coupler loss circuit model of an IPT system.

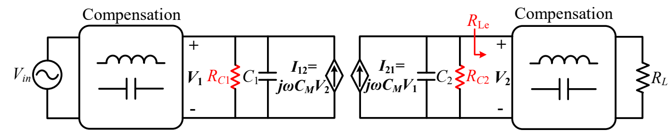

Fig.6. Coupler loss circuit model of a CPT system.

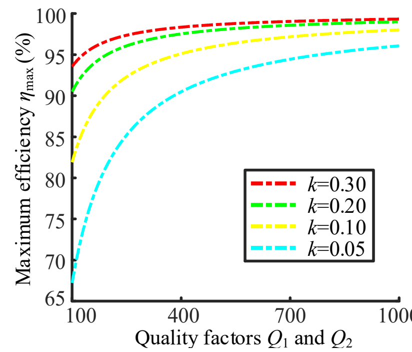

Fig.7. Transfer efficiency of IPT or CPT coupler versus k, Q_1 and Q_2

inductive or capacitive coupler but are also suitable for estimating the efficiency of the entire IPT and CPT system [29], in which the quality factors of primary and secondary circuits will be used instead of the quality factors of the pure coupler.

3) Maximum Efficiency Performance

A general form of the maximum efficiency for IPT and CPT couplers is provided in (18) when a_L=a_C=a_{max}, where k, Q_1, and Q_2 satisfy k=k_L=k_C, Q_1=Q_{L1}=Q_{C1}, Q_2=Q_{L2}=Q_{C2}.

$$\eta_{max}=\frac{k^2Q_1Q_2}{(1+\sqrt{1+k^2Q_1Q_2})^2},\ \ a_{max}=\sqrt{1+k^2Q_1Q_2} \quad (18)$$

The theoretical maximum transfer efficiency of capacitive or inductive coupler versus coupling coefficient and quality factor is shown in Fig.7, which shows a positive relationship between k and Q_1/Q_2 and can guide the system parameter design. For example, with estimated quality factors Q_1 and Q_2 of 400, to achieve an ac-ac efficiency of 95%, the coupling coefficient k can not be smaller than 0.1. Meantime, with k=0.2 and Q_1=Q_2=300, the maximum efficiency can only achieve 96.7%.

III. Duality Between Basic IPT and CPT Compensations

A. Comparison of Basic IPT and CPT Compensations

To achieve effective power transfer, double-sided compensation circuits are required to suppress the reactive power Q_{12}, making phase angle θ_{12} or φ_{21} close to 90°. For both IPT and CPT couplers, there are four basic compensations, namely, SS, PP, SP, and PS, compared in Tables VI and VII.

Particularly, z, y, h, and g-parameters are respectively suitable for SS, PP, SP, and PS circuits. Then, in the equivalent circuit, inductors and capacitors construct either series or parallel LC tanks. With such a configuration, it is straightforward to conclude the resonance relationship of the circuit by making the series/parallel LC tanks fully resonate, facilitating the circuit resonance analysis.

This article has been accepted for publication in IEEE Transactions on Transportation Electrification. This is the author's version which has not been fully edited and content may change prior to final publication. Citation information: DOI 10.1109/TTE.2022.3225578

Table VI Four basic IPT compensation circuits.

SS IPT Compensation [11]	PP IPT Compensation [12]	SP IPT Compensation [13]	PS IPT Compensation [14]
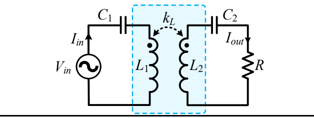	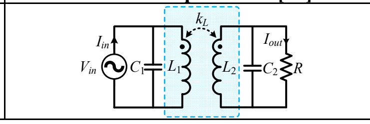	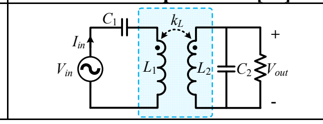	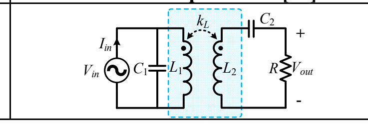
Behavior-source circuit			
z-parameter model	*y*-parameter model	*h*-parameter model	*g*-parameters model
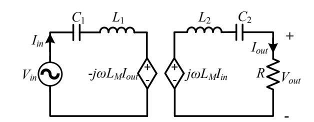	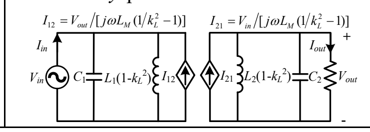	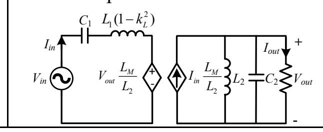	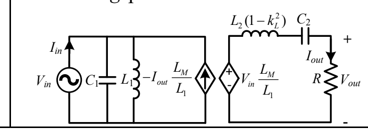
ZPA frequency			
$\omega_0=\frac{1}{\sqrt{L_1C_1}}=\frac{1}{\sqrt{L_2C_2}}$	$\omega_0=\frac{1}{\sqrt{L_1C_1(1-k_L^2)}}=\frac{1}{\sqrt{L_2C_2(1-k_L^2)}}$	$\omega_0=\frac{1}{\sqrt{L_1C_1(1-k_L^2)}}=\frac{1}{\sqrt{L_2C_2}}$	$\omega_0=\frac{1}{\sqrt{L_1C_1}}=\frac{1}{\sqrt{L_2C_2(1-k_L^2)}}$
Phase angle θ_{12} at ZPA frequency			
θ_{12}=90° (Q_{12}=0)	90°<θ_{12}<180°	90°<θ_{12}<180°	90°<θ_{12}<180°
Output Property at voltage source			
$I_{out}=-V_{in}/(j\omega_0L_M)$ (CC)	$I_{out}=V_{in}/[j\omega_0L_M(1/k_L^2-1)]$ (CC)	$V_{out}=V_{in}\cdot L_2/L_M$ (CV)	$V_{out}=V_{in}\cdot L_M/L_1$ (CV)
Output Property at current source			
$V_{out}=I_{in}j\omega_0L_M$ (CV)	$V_{out}=-I_{in}\cdot j\omega_0L_M(1/k_L^2-1)$ (CV)	$I_{out}=I_{in}\cdot L_M/L_2$ (CC)	$I_{out}=I_{in}\cdot L_1/L_M$ (CC)

Table VII Four basic CPT compensation circuits.

SS CPT Compensation [15]	PP CPT Compensation [16]	SP CPT Compensation [17]	PS CPT Compensation [18]
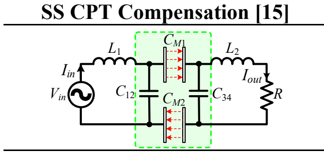	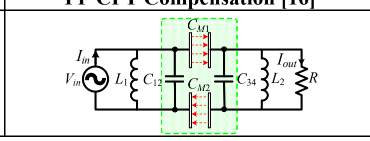	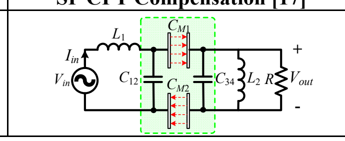	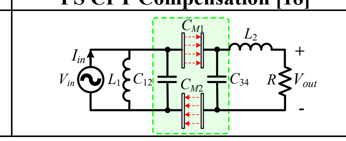
Behavior-source circuit			
z-parameter model	*y*-parameter model	*h*-parameter model	*g*-parameters model
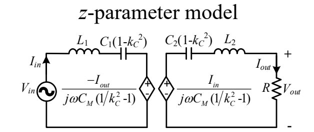	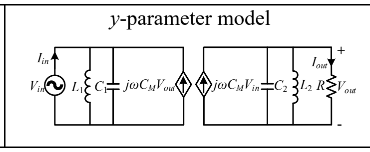	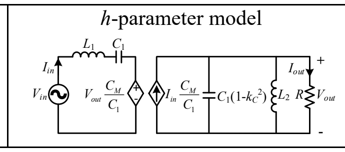	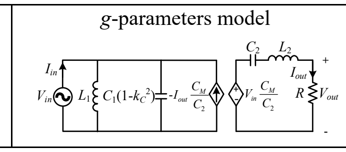
ZPA frequency			
$\omega_0=\frac{1}{\sqrt{L_1C_1(1-k_C^2)}}=\frac{1}{\sqrt{L_2C_2(1-k_C^2)}}$	$\omega_0=\frac{1}{\sqrt{L_1C_1}}=\frac{1}{\sqrt{L_2C_2}}$	$\omega_0=\frac{1}{\sqrt{L_1C_1}}=\frac{1}{\sqrt{L_2C_2(1-k_C^2)}}$	$\omega_0=\frac{1}{\sqrt{L_1C_1(1-k_C^2)}}=\frac{1}{\sqrt{L_2C_2}}$
Phase angle φ_{21} at ZPA			
0<φ_{21}<90°	φ_{21}=90° (Q_{12}=0)	0<φ_{21}<90°	0<φ_{21}<90°
Output Property at voltage source			
$I_{out}=-V_{in}j\omega_0C_M(1/k_C^2-1)$ (CC)	$I_{out}=V_{in}\cdot j\omega_0C_M$ (CC)	$V_{out}=V_{in}\cdot C_1/C_M$ (CV)	$V_{out}=V_{in}\cdot C_M/C_2$ (CV)
Output Property at current source			
$V_{out}=I_{in}/[j\omega_0C_M(1/k_C^2-1)]$ (CV)	$V_{out}=-I_{in}/(j\omega_0C_M)$ (CV)	$I_{out}=I_{in}\cdot C_M/C_1$ (CC)	$I_{out}=I_{in}\cdot C_2/C_M$ (CC)

1) SS Compensation

SS IPT/CPT compensation is compatible with the *z*-parameter modeling. At ZPA frequency, both SS IPT and CPT circuits realize the conversion between CC and CV properties. In an SS IPT circuit, the ZPA frequency is independent of k_L while in the SS CPT circuit, the ZPA frequency depends on k_C.

2) PP Compensation

PP IPT/CPT compensation is compatible with *y*-parameter modeling, and they can also achieve conversion between CC and CV properties. In a PP IPT circuit, ZPA frequency is related to k_L, while in a PP CPT circuit, ZPA frequency is independent of k_C.

3) SP Compensation

SP IPT/CPT compensation is compatible with the *h*-parameters. Both SP IPT and CPT circuits work as a step-up "transformer", which can boost the output voltage. For an SP IPT circuit, the conversion ratio is determined by L_2/L_M, while in an SP CPT circuit, the ratio is determined by C_2/C_M.

4) PS Compensation

PS IPT/CPT compensation is compatible with the *g*-parameters. Both SP IPT and CPT circuits work as a step-down "transformer", which decreases the output. In a PS IPT circuit, the voltage conversion ratio is determined by L_M/L_1 while in the PS CPT circuit, the ratio is determined by C_M/C_1.

According to (4) and (8), when θ_{12} or φ_{21} achieves 90°, there is no reactive power circulation Q_{12} within coupler, which helps reduce power loss on the coupler and maximize the active power transfer P_{12}. In an IPT system, θ_{21}=90° is only achievable in an SS compensation, which makes the SS IPT circuit the optimal one. In a CPT system, φ_{21}=90° is only achievable in a PP CPT compensation. However, in a PP CPT topology, the port voltages V_1 and V_2 are directly limited by the practical input and output voltages, which are generally in

This article has been accepted for publication in IEEE Transactions on Transportation Electrification. This is the author's version which has not been fully edited and content may change prior to final publication. Citation information: DOI 10.1109/TTE.2022.3225578

hundreds of volts, resulting in a low power transfer capability. Therefore, in practice, a pure PP CPT circuit is rarely adopted.

B. Duality Between Basic IPT and CPT Topologies

According to Tables VI and VII, the duality between basic IPT and CPT compensations exists in two aspects.

First, compensation circuit configuration. The SS, PP, SP, and PS CPT topologies respectively have identical compensation configuration, two-port modeling, load-independent output property, and inversion and rectification requirements as their IPT counterparts, namely SS, PP, SP, and PS ones. For example, both SS IPT and SS CPT configure the compensation component in series connection with the inductive/capacitive coupler, show compatibility with two-port *z*-parameter modeling, achieve load-independent CC output, and require voltage-source inverter (VSI) and voltage-source rectifier (VSR). Such duality can also be found in PP, SP, and PS-type IPT and CPT topologies. In summary, with the duality in compensation circuit configuration, the series (S) and parallel (P) compensation capacitors in an IPT circuit respectively correspond to the series (S) and parallel (P) compensation inductor in a CPT circuit.

Second, resonant relationship. In four basic IPT compensations, SS is considered the optimal one because its resonant frequency is independent of the coupling coefficient and there is no reactive power circulating in the inductive coupler in resonant conditions. In the CPT system, similar merits only exist in PP CPT compensation, not the SS one. From this perspective, PP CPT compensation is the counterpart of SS CPT. Similarly, PP, SP, and PS-type IPT compensations show similarity with SS, PS, and SP-type CPT circuits in the resonant relationship, respectively. Therefore, considering duality of resonance, the series (S) and parallel (P) compensation capacitors in an IPT circuit respectively correspond to the parallel (P) and series (S) compensation inductor in a CPT circuit.

In summary, CPT technology could be considered a reflection of IPT in a special "mirror", hence the name "duality" between IPT and CPT systems in this paper. The duality between IPT and CPT compensations, qualitatively and quantitatively, is summarized in Tables VIII and IX. Each IPT topology can find two counterparts of the CPT field in terms of compensation circuit configuration and resonant relationship, helping explore potential CPT circuits.

Table VIII Duality between SS- and PP-type IPT and CPT compensations.

CPT Topology / IPT Topology	**Series-Series CPT** 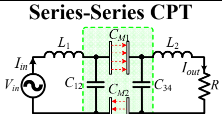	**Parallel-Parallel CPT** 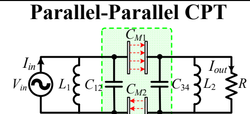
Series-Series IPT 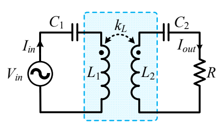	**Similarity in compensation circuit configuration** • Double-sided series compensation circuit • Two-port *z*-parameter modeling • Load-independent CC output • VSI and VSR required (1)	**Similarity in resonant relationship** • *k*-independent resonance: $\omega_0=\frac{1}{\sqrt{L_1C_1}}=\frac{1}{\sqrt{L_2C_2}}$ • Zero reactive power flow Q_{12}=0 ($\theta_{12}=\varphi_{12}$=90°) • L_M and C_M-dependent output: $\begin{cases} I_{out}\|_{SS-IPT}=j\cdot V_{in}/\omega L_M \\ I_{out}\|_{PP-CPT}=j\cdot V_{in}\omega C_M \end{cases}$
Parallel-Parallel IPT 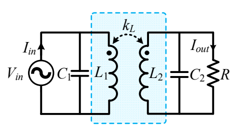	**Similarity in resonant relationship** • *k*-dependent resonance: $\omega_0=\frac{1}{\sqrt{L_1C_1(1-k^2)}}=\frac{1}{\sqrt{L_2C_2(1-k^2)}}$ • Non-zero reactive power flow $Q_{12}\neq 0$ • CC output expression: $\begin{cases} I_{out}\|_{PP-IPT}=I_{out}\|_{PP-CPT}\div(1-1/k_L^2) \\ I_{out}\|_{SS-CPT}=I_{out}\|_{PP-CPT}\times(1-1/k_C^2) \end{cases}$	**Similarity in compensation circuit configuration** • Double-sided parallel compensation circuit • Two-port *y*-parameter modeling • Load-independent CC output • CSI and CSR required (2)

(1) VSI: voltage-source inverter; VSR: voltage-source rectifier; (2) CSI: Current-source inverter; CSR: Current-source rectifier

Table IX Duality between SP- and PS-type IPT and CPT compensations.

CPT Topology / IPT Topology	**Series-Parallel CPT** 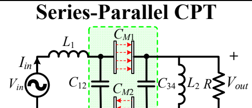	**Parallel-Series CPT** 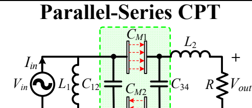
Series-Parallel IPT 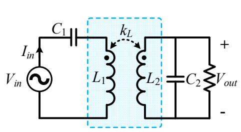	**Similarity in compensation circuit configuration** • Primary series and secondary parallel compensation circuit • Two-port *g*-parameter modeling • Load-independent step-up CV output • VSI and CSR required	**Similarity in resonant relationship** • *k*-independent resonance: $\omega_0=\frac{1}{\sqrt{L_1C_1(1-k^2)}}=\frac{1}{\sqrt{L_2C_2}}$ • Non-zero reactive power flow $Q_{12}\neq 0$ • L_1 and C_1-independent output: $\begin{cases} V_{out}\|_{SP-IPT}=V_{in}\cdot L_2/L_M \\ V_{out}\|_{PS-CPT}=V_{in}\cdot C_M/C_2 \end{cases}$
Parallel-Series IPT 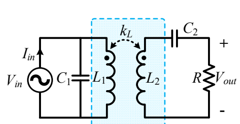	**Similarity in resonant relationship** • *k*-dependent resonance: $\omega_0=\frac{1}{\sqrt{L_1C_1}}=\frac{1}{\sqrt{L_2C_2(1-k^2)}}$ • Non-zero reactive power flow $Q_{12}\neq 0$ • L_2 and C_2-independent output: $\begin{cases} V_{out}\|_{PS-IPT}=V_{in}\cdot L_M/L_1 \\ V_{out}\|_{SP-CPT}=V_{in}\cdot C_1/C_M \end{cases}$	**Similarity in compensation circuit configuration** • Primary parallel and secondary series compensation circuit • Two-port *h*-parameter modeling • Load-independent step-down CV output • CSI and VSR required

This article has been accepted for publication in IEEE Transactions on Transportation Electrification. This is the author's version which has not been fully edited and content may change prior to final publication. Citation information: DOI 10.1109/TTE.2022.3225578

IV. Exploration of CPT Opportunities Based on Duality with Mainstream IPT Circuits

A. Exploration of CPT Opportunities

According to the aforementioned duality investigation, for any IPT topology, it is accessible to find two CPT counterparts based on the duality of compensation configuration and resonant relationship. IPT technology has become very mature after development of over 100 years. According to the literature, apart from the 4 basic IPT topologies (SS, PP, SP, and PS), 7 higher-order IPT compensations, S-SP, LCC-S, LCC-P, LCC-SP, LCC-LCC, three-coil, and four-coil [30]-[36], are most commonly researched and used, which can be considered as the optimal IPT circuit candidates. Based on the duality with the existing 7 optimal IPT circuits, 14 CPT topologies are derived, which possibly have good performance as well. Among these 14 CPT circuits, 3 have been reported in [25]-[27], namely, *LCL-S*, *LCL-LCL*, and M_1-*SS*-M_2 CPT circuits, which are the counterparts of LCC-LCC, LCC-S, and four-coils IPT circuits; however, the rest are not and are explored in detail as the following, and the comparison between IPT circuits and their counterparts are provided in Table X.

1) Duality with S-SP IPT Circuit: The S-SP compensated IPT [30] circuit is developed from the basic SP compensation. With an additional series capacitor at the secondary side, an S-SP IPT circuit can be designed in either voltage step-up or -down mode, achieving more flexible control of output voltage.

Table X. CPT Circuit Prediction based on the duality with IPT circuit.

Existing IPT Topology	Resonance	CPT Counterpart	Resonance
1.0 *S-SP* IPT Circuit [30]		**1.1 *S-SP* CPT Circuit (New)**	
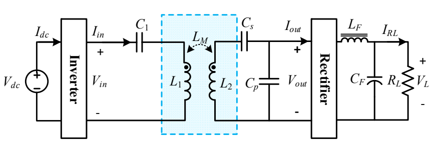	$L_2^* = L_2 - 1/(\omega^2 C_s)$ $\omega^2 (L_1 - \frac{L_M^2}{L_2^*}) C_1 = 1$ $\omega^2 L_2^* C_2 = 1$	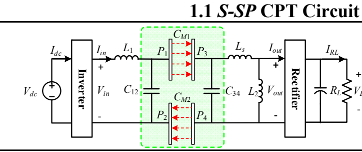	$L_2^* = L_2 + L_s$ $\frac{\omega^2 L_1 C_1 \cdot (1-k_C^2)}{1-(L_2^*/L_2)\cdot k_C^2} = 1$ $\omega^2 L_2^* C_2 (1-k_C^2) = 1$
		CV output: $V_{out} = V_{in} \frac{C_1}{C_M} \cdot \frac{L_2}{L_2^*}$ (φ_{21}<90°)	
		1.2 *P-PS* CPT Circuit (New)	
		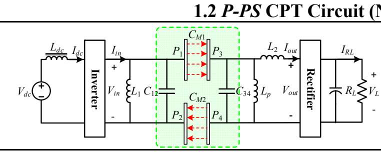	$C_2^* = C_2 - 1/(\omega^2 L_p)$ $\omega^2 (C_1 - \frac{C_M^2}{C_2^*}) L_1 = 1$ $\omega^2 L_2 C_2^* = 1$
CV output: $V_{out} = V_{in} \cdot \frac{L_2^*}{L_M}$		CV output: $V_{out} = V_{in} \frac{C_M}{C_2^*}$ (φ_{21}<90°)	
2.0 *LCC-S* IPT Circuit (*LCL-S/S* Compensation) [31]		**2.1 *LCL-S* CPT Circuit** (*LCL-S/S* Compensation) **[25]**	
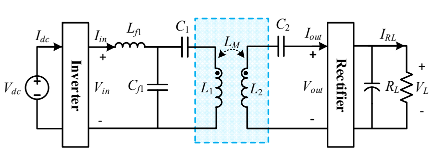	$\omega^2 L_{f1} C_{f1} = 1$ $\omega^2 (L_1 - L_{f1}) C_1 = 1$ $\omega^2 L_2 C_2 = 1$	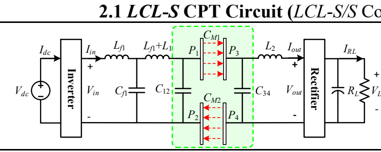	$\omega^2 L_{f1} C_{f1} = 1$ $\omega^2 L_1 C_1 (1-k_C^2) = 1$ $\omega^2 L_2 C_2 (1-k_C^2) = 1$
		CV output: $V_{out} = -V_{in} \cdot \frac{C_{f1}}{C_M} \cdot \frac{k_C^2}{1-k_C^2}$ (φ_{21}<90°)	
		2.2 *CLC-P* CPT Circuit (*CLC-P/P* Compensation) **(New)**	
		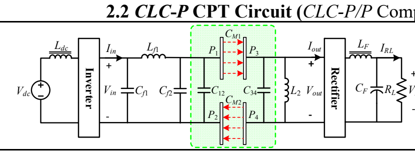	$\omega^2 L_{f1} C_{f1} = 1$ $\omega^2 L_2 C_2 = 1$ $C_{f2} = C_{f1} - C_1$
CV output: $V_{out} = V_{in} \frac{L_M}{L_{f1}}$		CV output: $V_{out} = V_{in} \cdot \frac{C_{f1}}{C_M}$ (φ_{21}=90°)	
3.0 *LCC-P* IPT Circuit (*LCL-S/P* Compensation) [32]		**3.1 *LCL-P* CPT Circuit** (*LCL-S/P* Compensation) **(New)**	
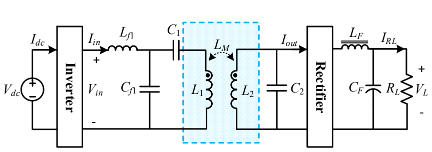	$\omega^2 L_{f1} C_{f1} = 1$ $\omega^2 (L_1 - L_{f1} - \frac{L_M^2}{L_2}) C_1 = 1$ $\omega^2 L_2 C_2 = 1$	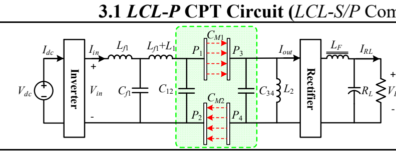	$\omega^2 L_{f1} C_{f1} = 1$ $\omega^2 L_1 C_1 = 1$ $\omega^2 L_2 C_2 (1-k_C^2) = 1$
		CC output: $I_{out} = -V_{in} j\omega C_{f1} \cdot \frac{C_M}{C_1}$ (φ_{21}<90°)	
		3.2 *CLC-S* CPT Circuit (*CLC-P/S* Compensation) **(New)**	
		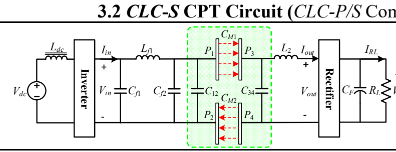	$\omega^2 L_{f1} C_{f1} = 1$ $\omega^2 L_2 C_2 = 1$ $C_{f2} = C_{f1} - C_1 (1-k_C^2)$
CC output: $I_{out} = \frac{V_{in}}{j\omega L_{f1}} \cdot \frac{L_M}{L_2}$		CC output: $I_{out} = -V_{in} j\omega C_{f1} \cdot \frac{C_2}{C_M}$ (φ_{21}<90°)	

Continuous next page

This article has been accepted for publication in IEEE Transactions on Transportation Electrification. This is the author's version which has not been fully edited and content may change prior to final publication. Citation information: DOI 10.1109/TTE.2022.3225578

4.0 *LCC-SP* IPT Circuit (*LCL-S/SP* Compensation) [33]

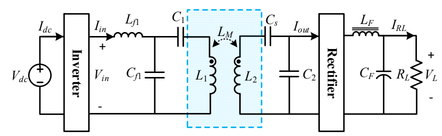

$$\begin{cases} \omega^2 L_{f1} C_{f1} = 1 \\ L_2^* = L_2 - 1/(\omega^2 C_s) \\ \omega^2 (L_1 - L_{f1} - \frac{L_M^2}{L_2^*}) C_1 = 1 \\ \omega^2 L_2^* C_2 = 1 \end{cases}$$

CC output: $I_{out} = \dfrac{V_{in}}{j\omega L_{f1}} \cdot \dfrac{L_M}{L_2^*}$

4.1 *LCL-SP* CPT Circuit (*LCL-S/SP* Compensation) **(New)**

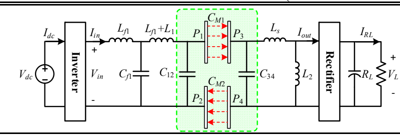

$$\begin{cases} \omega^2 L_{f1} C_{f1} = 1 \\ L_2^* = L_2 + L_s \\ \dfrac{\omega^2 L_1 C_1 \cdot (1-k_C^2)}{1-(L_2^*/L_2)\cdot k_C^2} = 1 \\ \omega^2 L_2^* C_2 (1-k_C^2) = 1 \end{cases}$$

CC output: $I_{out} = -V_{in} j\omega C_{f1} \cdot \dfrac{C_M}{C_1} \cdot \dfrac{L_2^*}{L_2}$ (φ_{21}<90°)

4.2 *CLC-PS* CPT Circuit (*CLC-P/PS* Compensation) **(New)**

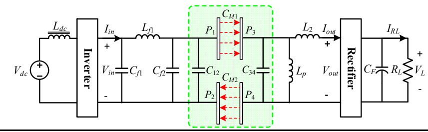

$$\begin{cases} \omega^2 L_{f1} C_{f1} = 1 \\ C_2^* = C_2 - 1/(\omega^2 L_p) \\ \omega^2 L_2 C_2^* = 1 \\ C_{f2} = C_{f1} - (C_1 - \frac{C_M^2}{C_2^*}) \end{cases}$$

CC output: $I_{out} = -V_{in} j\omega C_{f1} \cdot \dfrac{C_2^*}{C_M}$ (φ_{21}<90°)

5.0 Three-Coil IPT Circuit (M_1-*S/S* Compensation) [34]

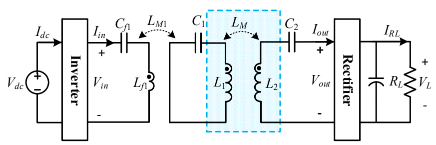

$$\begin{cases} \omega^2 L_{f1} C_{f1} = 1 \\ \omega^2 L_1 C_1 = 1 \\ \omega^2 L_2 C_2 = 1 \end{cases}$$

CV output: $V_{out} = V_{in} \dfrac{L_M}{L_{M1}}$ (Q_{12}=0)

5.1. M_1-*SS* CPT Circuit (M_1-*S/S* Compensation) (New)

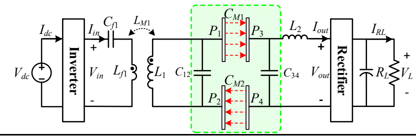

$$\begin{cases} \omega^2 L_{f1} C_{f1} = 1 \\ \omega^2 L_1 C_1 (1-k_C^2) = 1 \\ \omega^2 L_2 C_2 (1-k_C^2) = 1 \end{cases}$$

CV output: $V_{out} = \dfrac{V_{in}}{\omega^2 L_{M1} C_M (1/k_C^2 - 1)} = V_{in} \dfrac{L_1}{L_{M1}} \dfrac{C_M}{C_2}$ (φ_{21}<90°)

5.2 *LCL*-P CPT Circuit (M_1-*P/P* Compensation) **(New)**

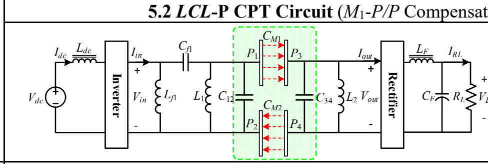

$$\begin{cases} \omega^2 L_{f1} C_{f1} = 1 \\ \omega^2 L_1 (C_1 + C_{f1}) = 1 \\ \omega^2 L_2 C_2 = 1 \end{cases}$$

CV output: $V_{out} = -V_{in} \dfrac{C_{f1}}{C_M}$ (φ_{21}=90°)

6.0 *LCC-LCC* IPT Circuit (*LCL-S/S-LCL* compensation) [35]

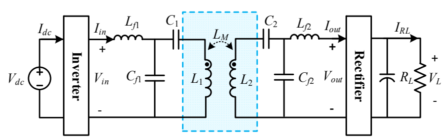

$$\begin{cases} \omega^2 L_{f1} C_{f1} = 1 \\ \omega^2 L_{f2} C_{f2} = 1 \\ \omega^2 (L_1 - L_{f1}) C_1 = 1 \\ \omega^2 (L_2 - L_{f2}) C_2 = 1 \end{cases}$$

CC output: $I_{out} = \dfrac{V_{in} L_M}{j\omega L_{f1} L_{f2}}$ (Q_{12}=0)

6.1. *LCL-LCL* CPT Circuit (*LCL-S/S-LCL* compensation) [26]

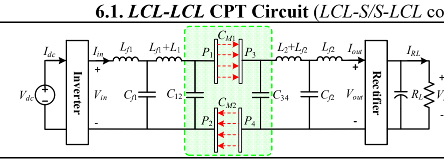

$$\begin{cases} \omega^2 L_{f1} C_{f1} = 1 \\ \omega^2 L_{f2} C_{f2} = 1 \\ \omega^2 L_1 C_1 (1-k_C^2) = 1 \\ \omega^2 L_2 C_2 (1-k_C^2) = 1 \end{cases}$$

CC output: $I_{out} = V_{in} \cdot \dfrac{j\omega C_{f1} C_{f2}}{C_M} \cdot \dfrac{k_C^2}{1-k_C^2}$ (φ_{21}<90°)

6.2 *CLC-CLC* CPT Circuit (*CLC-P/P-CLC* compensation) **(New)**

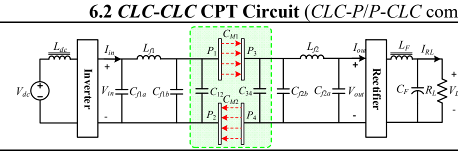

$$\begin{cases} \omega^2 L_{f1} C_{f1a} = 1 \\ \omega^2 L_{f2} C_{f2a} = 1 \\ C_{f1b} = C_{f1a} - C_1 \\ C_{f2b} = C_{f2a} - C_2 \end{cases}$$

CC output: $I_{out} = -V_{in} \dfrac{j\omega C_{f1a} C_{f2a}}{C_M}$ (φ_{21}=90°)

7.0 Four-Coil IPT Circuit (M_1-*S/S*-M_2 Compensation) [36]

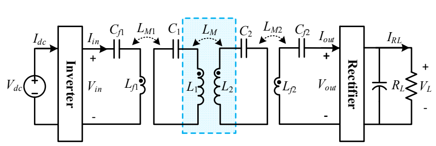

$$\begin{cases} \omega^2 L_{f1} C_{f1} = 1 \\ \omega^2 L_{f2} C_{f2} = 1 \\ \omega^2 L_1 C_1 = 1 \\ \omega^2 L_2 C_2 = 1 \end{cases}$$

CC output: $I_{out} = \dfrac{V_{in} L_M}{j\omega L_{M1} L_{M2}}$ (Q_{12}=0)

7.1 M_1-*SS*-M_2 CPT circuit (M_1-*S/S*-M_2 Compensation) [27]

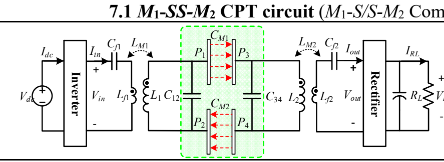

$$\begin{cases} \omega^2 L_{f1} C_{f1} = 1 \\ \omega^2 L_{f2} C_{f2} = 1 \\ \omega^2 L_1 C_1 (1-k_C^2) = 1 \\ \omega^2 L_2 C_2 (1-k_C^2) = 1 \end{cases}$$

CC output: $I_{out} = \dfrac{-V_{in}}{j\omega^3 L_{M1} L_{M2} C_M} \cdot \dfrac{k_C^2}{1-k_C^2}$ (φ_{21}<90°)

7.2 *LCL-PP-LCL* CPT Circuit (*LCL-P/P-LCL* Compensation) **(New)**

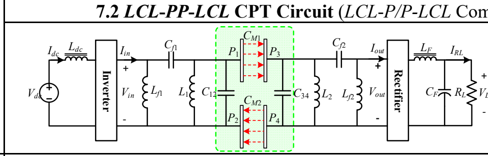

$$\begin{cases} \omega^2 L_{f1} C_{f1} = 1 \\ \omega^2 L_{f2} C_{f2} = 1 \\ \omega^2 L_1 (C_1 + C_{f1}) = 1 \\ \omega^2 L_2 (C_2 + C_{f2}) = 1 \end{cases}$$

CC output: $I_{out} = -V_{in} \dfrac{j\omega C_{f1} C_{f2}}{C_M}$ (φ_{21}=90°)

Considering the duality in circuit structure, an S-SP compensated CPT circuit is proposed, shown as case 1.1 in Table X. Compared to the basic SP CPT circuit, one more compensation inductor is used, however, the total net inductance on the secondary side does not increase. Meantime, it can also be designed in voltage step-up or -down mode.

Considering the duality in the resonant relationship, a *P-PS* compensated CPT circuit is proposed with flexible voltage step-down/up output, shown as case 1.2 in Table X. However, according to the resonant relationship, in the P-PS CPT circuit, the secondary-side net inductance increases compared to a PS CPT circuit, which is a drawback.

2) Duality with LCC-S IPT Circuit: The *LCC-S* IPT circuit [31] is equivalent to a combination of a primary-side T-type *LCL* network and an SS IPT compensation. The second inductor of the *LCL* network is canceled by the series capacitor of the SS circuit, resulting in an *LCC-S* IPT system. *LCC-S* is a classic IPT topology, which achieves constant transmitting current, load-independent CV output, and zero reactive power circulation in the magnetic coupler with a compact receiver.

Considering the duality of circuit configuration with *LCC*-S IPT, the *LCL-S* CPT circuit is developed, shown as case 2.1 in Table X. It can achieve load-independent CV output with a compact receiver circuit, which has been reported in [25].

Considering the resonant relationship, the SS IPT is in duality with PP CPT. Similarly, the T-type *LCL* network should be in duality with a Π-type *CLC* network [37]. Therefore, a *CLC-P* CPT circuit is developed as case 2.2 in Table X, in which the second capacitor of the Π-type *CLC* network cancels the primary compensation inductor of the PP CPT circuit. For the *CLC-P* CPT circuit, zero reactive power circulation (Q_{12}=0) is achieved, and only two resonant inductors are required. However, the secondary port voltage V_2 of the coupler is limited by the load voltage, which is adverse for high power transfer. Besides, the *CLC-P* CPT circuit requires a current-source inverter.

3) Duality with LCC-P IPT Circuit: The *LCC-P* IPT circuit [32] can be considered as a combination of a T-type *LCL* network and a basic SP IPT circuit. The secondary inductor of the *LCL* network is canceled by the series capacitor of an SP IPT circuit. It achieves CC output with a compact receiver.

Considering the duality, *LCL-P* and *CLC-S* CPT circuits are respectively developed with CC output, shown in cases 3.1 and 3.2 in Table X. For the *LCL-P* CPT circuit, port voltage V_2 of the capacitive coupler is limited by the load voltage, which is adverse for high power transfer. In comparison, the CLC-S CPT circuit uses fewer resonant inductors and overcomes the drawback of the *LCL-P* CPT circuit.

4) Duality with LCC-SP IPT Circuit: The *LCC-SP* IPT circuit [33] is an improved version of the *LCC-P* IPT circuit, using an additional series capacitor at the secondary side to achieve more design flexibility.

Considering the duality, *LCL-SP* and *CLC-PS* CPT circuits are respectively developed, shown in cases 4.1 and 4.2. The *LC*L-*SP* CPT circuit is an improved version of the *LCL-P* CPT circuit (case 3.1), which can boost the secondary port voltage V_2 without increasing the secondary net inductance. In contrast, the *CLC-PS* circuit does not improve when compared to the *CLC-S* CPT circuit (case 3.2).

5) Duality with Three-Coil IPT Circuit: In the three-coil IPT circuit [34], a mutually coupled magnetic-link is used at the primary side, which works as a CC excitation for the followed SS CPT circuit. In this case, a CV output property is achieved when neglecting the cross-coupling.

Considering the duality in circuit configuration, an M_1-*SS* CPT circuit is developed, shown as case 6.1. Considering the resonant relationship, the SS mutually coupled magnetic-link is in duality with the Π-type *LCL* network [37]. Hence the *LCL-PP* CPT circuit is developed as case 6.2. Similarly, in the *LCL-PP* CPT circuit, the coupler port voltage V_2 is limited by load voltage, which is adverse for high power transfer.

6) Duality with LCC-LCC IPT Circuit: LCC-LCC IPT circuit [35] is one of the most classic topologies, which is equivalent to the combination of a double-side T-type LCL network and an SS IPT compensation. It achieves CC output, constant transmitting current, and zero reactive power circulation.

Considering the duality, *LCL-LCL* and *CLC-CLC* CPT circuits are respectively developed. The *LCL-LCL* CPT circuit has been validated to achieve a high power of 2.4kW with over 90% efficiency [26]. In comparison, the newly proposed *CLC-CLC* CPT topology requires fewer resonant inductors. Meantime, the property of zero reactive power circulation potentially helps to further improve system efficiency. The *CLC-CLC* CPT circuit requires the current-source inverter and rectifier.

7) *Duality with Four-Coil IPT Circuit:* The four-coil IPT circuit [36] uses two additional mutually coupled magnetic links on double sides, which have a similar function to a T-type *LCL*/*CLC* network. The main coupling is designed as an SS circuit. Neglecting cross-couplings, CC output is achieved.

Considering the duality in circuit configuration, the M_1-*SS*-M_2 and *LCL-PP-LCL* CPT circuits are respectively developed as cases 7.1 and 7.2. M_1-*SS*-M_2 CPT circuit has been validated in [27], which achieves a high power of 3kW and an efficiency of up to 95.7%. In comparison, the newly proposed *LCL-PP-LCL* CPT circuit can achieve zero reactive power circulation in the capacitive coupler, which is a potential merit.

B. Evaluation of Developed CPT Circuits

Based on the duality investigation with 7 mainstream higher-order IPT circuits, 14 CPT circuits are developed. Particularly, 11 of these 14 CPT circuits are newly proposed in this paper. Table X marks all 14 circuits and indicates the ones already in literature and the ones explored in this paper.

In comparison, the four basic CPT topologies, SS, PP, SP and PS, have the simplest circuit structure and are more suitable for low-power applications. However, the newly developed 14 high-order CPT circuits tend to achieve more design flexibility and freedom for high power transfer capability and load-independent CC or CV output property, which can be selectively used for different scenarios. For example, the newly proposed *S-SP* CPT circuit permits a more flexible CV output design (either step-up or step-down) than the basic SP CPT that can only achieve voltage step-up. Besides, in the *LCL-LCL* CPT circuit, with the double-side *LCL* networks, additional two variables C_{f1} and C_{f2} are introduced, which can be leveraged to increase the system power level, meaning higher design flexibility. Table XI provides a summary and evaluation of the developed 14 CPT circuits in terms of inver-

Table XI Summary and evaluation of the derived 14 high-order CPT circuits.

CPT Circuit	Inverter and Rectifier	Compensation Inductor Num.	Compensation Capacitor Num.	Output Property	Circuit Simplicity	Power Transfer Capability	Recommendation
1.1 *S-SP* CPT	VSI, VSR	3	0	CV	★★★★	Low	✓
1.2 *P-PS* CPT	CSI, VSR	3	0	CV	★★★☆	Low	×
2.1 *LCL-S* CPT [25]	VSI, VSR	3	1	CV	★★★	Medium	✓
2.2 *CLC-P* CPT	CSI, CSR	2	1	CV	★★★	Low	×
3.1 *LCL-P* CPT	VSI, CSR	3	1	CC	★★★	Low	×
3.2 *CLC-S* CPT	CSI, VSR	2	2	CC	★★★	Medium	✓
4.1 *LCL-SP* CPT	VSI, VSR	4	1	CC	★★☆	Medium	✓
4.2 *CLC-PS* CPT	CSI, VSR	3	2	CC	★★☆	Medium	✓
5.1. M_1-SS CPT	VSI, VSR	3	2	CV	★★★	Medium	✓
5.2 *LCL*-P CPT	CSI, CSR	3	2	CV	★★☆	Low	×
6.1. *LCL-LCL* CPT [26]	VSI, VSR	4	2	CC	★★	High	✓
6.2 *CLC-CLC* CPT	CSI, CSR	2	4	CC	★★	High	✓
7.1 M_1-*SS*-M_2 CPT [27]	VSI, VSR	4	2	CC	★★	High	✓
7.2 *LCL-PP-LCL* CPT	CSI, CSR	4	2	CC	★★	High	✓

sion and rectification design, the number of compensation components, output property, circuit simplicity, and power transfer capability.

Compared to basic CPT compensations, the *S-SP* and *P-PS* CPT circuits use only one more inductor on the secondary side to achieve a more flexible output voltage, which has a relatively compact system size and low power transfer capability. However, the *P-PS* CPT circuit requires larger secondary-side inductance than the *S-SP* circuit, and therefore, is not recommended.

For the CPT circuits of cases 2.1~5.2 in Table XI, a T-type *LCL* or Π-type *CLC* network is used in the primary side when compared to the basic CPT circuits, which introduces additional design degrees of freedom for improving power transfer capability without significantly increasing the complexity of the secondary circuit. There are exceptions, however. For example, in the *CLC-P*, *LCL-P*, and *LCL-P* CPT circuits, the port voltage V_2 of the capacitive coupler will be limited by the load voltage to hundreds of volts, which is adverse for high power transfer. Therefore, these circuits are not recommended.

For the CPT circuits of cases 6.1~7.2, double-sided T-type *LCL* or Π-type *CLC* networks are used, which introduces two more design degrees for a high power transfer capability at the cost of increased circuit complexity, which are mainly expected to be applied to high-power scenarios.

In summary, compared to the 4 basic CPT circuits, some of the new circuits clearly show 1) potentials of flexible output, such as *S-SP*; 2) trade-off between circuit simplicity and power transfer capability, such as *LCL-S,* and M_1-*SS*; and 3) high power transfer capability, such as M_1-*SS*-M_2, and *LCL-LCL* which can be selectively used in various scenarios, such as electric vehicle charging, underwater capacitive power transfer, etc.

V. Case Study with Experiment Validation

A. Validation from the Existing Work

Based on the presented duality analysis, 14 CPT topologies are derived from 7 mainstream IPT circuits. Their performance in terms of resonant relationship, output property, and output power expressions are predicted. To validate the demonstrated duality analysis, the convincing approach is to experimentally verify the performance of the newly proposed CPT circuits with the prediction.

Among these 14 CPT circuits, the *LCL-S*, *LCL-LCL*, and M_1-*SS*-M_2 topologies have been respectively reported and investigated in [25], [26], and [27]. The existing research shows that the *LCL-S*, *LCL-LCL*, and M_1-*SS*-M_2 CPT circuits respectively achieve load-independent CV, CC, and CC output property. The resonant relationship and output power expressions are the same as predicted in this paper, which can validate the effectiveness of the proposed duality investigation in exploring high-performance CPT circuits.

B. Case Study of M_1*-SS CPT Circuit*

Beyond the existing related research, in this paper the M_1-*SS* CPT circuit (case 5.1), which uses a mutually coupling magnetic link on the primary side to improve the power transfer capability and only uses one inductor on the secondary side to achieve a compact receiver, is implemented to further validate the revealed duality between IPT and CPT systems.

The simplified M_1-*SS* CPT circuit is shown in Fig. 8. C_{M1} and C_{M2} are the main coupled capacitances while C_{12} and C_{34} are the parasitic shunt capacitance of the capacitive coupler. C_{ex1} and C_{ex2} are external capacitances. The coupler is described as:

$$\begin{cases} C_M = C_{M1}\cdot C_{M2}/(C_{M1}+C_{M2}) \\ C_1 = C_{ex1}+C_{12}+C_M,\ \ C_2 = C_{ex2}+C_{34}+C_M \end{cases} \tag{19}$$

z-parameter is used to simplify the system. The equivalent circuit is provided in Fig. 9, and resonant relationship satisfies

$$\omega = \frac{1}{\sqrt{L_{f1}C_{f1}}} = \frac{1}{\sqrt{L_1C_1(1-k_C^2)}} = \frac{1}{\sqrt{L_2C_2(1-k_C^2)}} \tag{20}$$

Based on the circuit, the voltage relationship is described as

$$\begin{cases} V_{in} = I_{in}\cdot(j\omega L_{f1}+\dfrac{1}{j\omega C_{f1}}) - I_{L1}j\omega L_{M1} \\ V_{out} = I_{L1}\dfrac{1}{j\omega C_M(1/k_C^2-1)} - I_{out}[j\omega L_2+\dfrac{1}{j\omega C_2(1-k_C^2)}] \end{cases} \tag{21}$$

The current I_{L1} is given below, which is independent of load, namely a CC excitation for the followed SS CPT circuit.

$$I_{L1} = -V_{in}/j\omega L_{M1} \tag{22}$$

The output voltage of the M_1-*SS* CPT is provided as

This article has been accepted for publication in IEEE Transactions on Transportation Electrification. This is the author's version which has not been fully edited and content may change prior to final publication. Citation information: DOI 10.1109/TTE.2022.3225578

$$V_{out}=\frac{V_{in}}{\omega^2 L_{M1}C_M(1/k_C^2-1)}=V_{in}\frac{L_1}{L_{M1}}\frac{C_M}{C_2} \quad (23)$$

C. 2.1kW 3MHz CPT Experiment

A 2.1kW CPT hardware prototype is implemented as shown in Fig. 10. A sleeve-type capacitive coupler is used, which can be usable in rotary applications [38]. With an air gap of 8mm, C_{M1} and C_{M2} achieve 50pF. A high frequency of 3MHz is selected. Silicon carbide MOSFET C3M0120100K is used to design the inverter, and 3000-strand AWG46 Litz wire is used to fabricate inductors. It is noted that in the implemented CPT system, the rectifier is not used. Multiple 2Ω/140W non-inductive resistors of OHMITE THE140 Series are connected as a high-power load. The system parameters are provided in Table XII.

With V_{dc}=300V, f=3MHz, and R=40Ω, the output power achieves 2.1kW and the experimental waveforms are provided in Fig. 11. The output voltage V_{out} is almost in phase with the input voltage V_{in}. Besides, the input current I_{in} only slightly lags V_{in} in phase, showing a ZPA property as well as zero-voltage-switching (ZVS), which reduces the switching loss.

The output voltage V_{out} and efficiency are provided in Fig. 12. When the power increases by 250% from 606W to 2122W, the output voltage only experiences a small decrease of 9.7% from 327.4V to 295.6V, validating the constant-voltage (CV) output. The small voltage fluctuation is attributed to the parasitic circuit resistance and the slight detuning for ZVS. The maximum efficiency reaches 93.19% at 755W and an efficiency of 89.8% is achieved at 2122W.

In this work, the purpose is to validate the feasibility of using the IPT-CPT duality for higher-order CPT exploration. In future work, high-quality components can be used to improve efficiency, and a high-frequency rectification stage will be implemented to achieve a dc output.

VI. Conclusion

This paper comparatively investigates the duality between CPT and IPT technologies, aiming at exploring the full suite of potential CPT opportunities not yet reported in the literature. The CPT and IPT systems are systematically compared in terms of modeling, power transfer mechanism, compensation circuit, resonant relationship, and power and efficiency. A generic two-port modeling method is developed, and unified power transfer and efficiency expressions are derived. The duality is demonstrated in aspects of compensation circuit configuration and resonant relationship. 14 CPT topologies are discovered in duality with 7 mainstream IPT circuits, of which 11 CPT circuits are not reported in the literature. Detailed comparison and evaluation of the developed 14 CPT circuits are conducted, and high-performance circuits are recommended. As a case study, a 2.1kW 3MHz CPT system is implemented in hardware based on the newly proposed M_1-SS CPT circuit which shows consistency with the predicted circuit properties of load-independent CV output, and ZPA property with a peak efficiency of 93.19%. The demonstrated experimental result and the existing research work in [25]-[27] jointly validate the proposed duality analysis. Design and hardware demonstration for the other theoretically-feasible CPT circuits is beyond the scope of the paper. However, this work paves a pathway for future researchers in this direction.

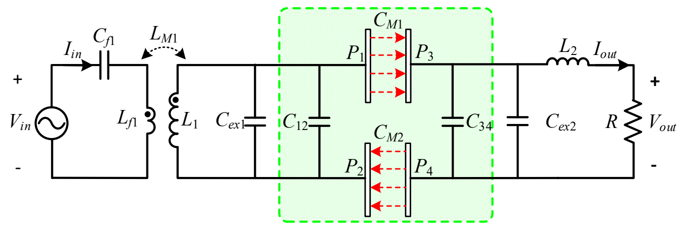

Fig.8 Circuit topology of M_1-SS CPT system.

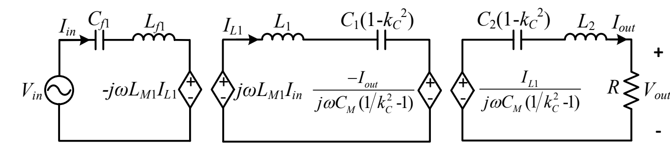

Fig.9 Equivalent circuit of M_1-SS CPT system based on z-parameter modeling.

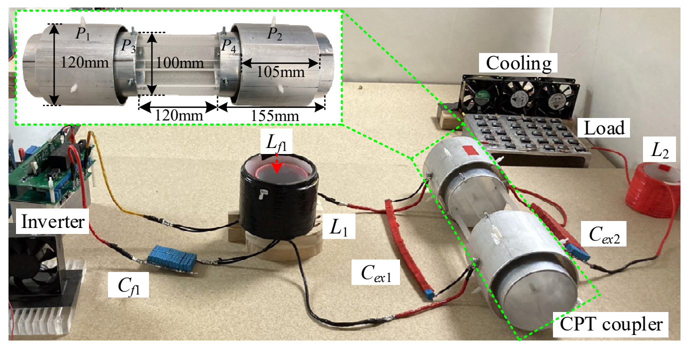

Fig.10 Implemented 2.1kW CPT prototype.

Table XII. Parameters of the implemented CPT prototype.

Parameter	Value	Parameter	Value
V_{dc}	300 V	f	3 MHz
L_{f1}	4.8 μH	C_{f1}	663.9 pF
L_1	70.0 μH	$C_{ex1}+C_{12}$	20.5 pF
L_2	27.0 μH	$C_{ex2}+C_{34}$	93.0pF
L_{M1}	13.6 μH	C_{M1}, C_{M2}	50.0pF
C_1	45.5 pF	C_2	118.0pF
C_M	25.0 pF	k_C	0.34
Air gap	8 mm	Voltage gain G_V	1.09

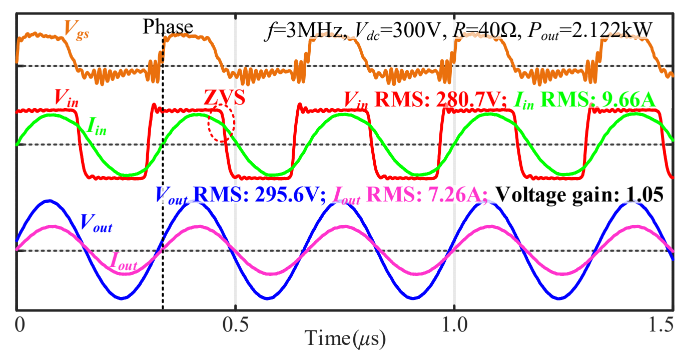

Fig.11 Experimental waveforms at 2.122kW and 3MHz.

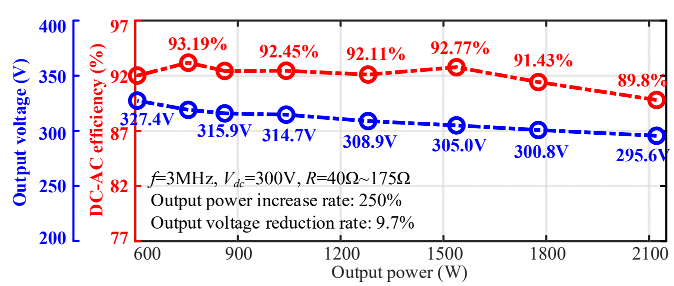

Fig.12 Output voltage and efficiency versus power.

ACKNOWLEDGMENT

The information, data, or work presented herein was funded in part by the Advanced Research Projects Agency-Energy (ARPA-E), U.S. Department of Energy, under Award Number DE-AR0001114 in the BREAKERS program monitored by Dr. Isik Kizilyalli. The views and opinions of authors expressed herein do not necessarily state or reflect those of the United States Government or any agency thereof.

REFERENCE

[1] S. Li, S. Lu and C. C. Mi, "Revolution of electric vehicle charging technologies accelerated by wide bandgap devices," *Proceedings of the IEEE*, vol. 109, no. 6, pp. 985-1003, June 2021.

[2] D. Patil, M. K. McDonough, J. M. Miller, B. Fahimi, *et al*., "Wireless power transfer for vehicular applications: overview and challenges," *IEEE Trans. Transport. Electrific.*, vol. 4, no. 1, pp. 3-37, March 2018.

[3] M. Mohammad, O. Onar, G. Su, J. Pries, V. Galigekere, S. Anwar, *et al*., "Bidirectional LCC–LCC-compensated 20-kW wireless power transfer system for medium-duty vehicle charging," *IEEE Trans. Transport. Electrific.*, vol. 7, no. 3, pp. 1205-1218, Sept. 2021.

[4] Society of Automotive Engineers. SAE J2954: wireless power transfer for light-duty plug-in/electric vehicles and alignment methodology. *SAE International*, 2019.

[5] H. Feng, R. Tavakoli, *et al*., "Advances in high-power wireless charging systems: overview and design considerations," *IEEE Trans. Transport. Electrific.*, vol. 6, no. 3, pp. 886-919, Sept. 2020.

[6] R. Tavakoli, *et al*, "Cost-Efficiency optimization of ground assemblies for dynamic wireless charging of electric vehicles," *IEEE Trans. Transport. Electrific*, vol. 8, no. 1, pp. 734-751, March 2022.

[7] V. -B. Vu, A. Ramezani, A. Triviño, et al., "Operation of inductive charging systems under misalignment conditions: a review for electric vehicles," *IEEE Trans. Transport. Electrific., Early Access*

[8] B. Zhang, J. Deng, W. Wang, L. Li, et al., "Multi-Objective thermal optimization based on improved analytical thermal models of a 30 kw IPT system for EVs," *IEEE Trans. Transport. Electrific.*, *Early Access*.

[9] S. Sinha, A. Kumar, B. Regensburger and K. K. Afridi, "A new design approach to mitigating the effect of parasitics in capacitive wireless power transfer systems for electric vehicle charging," *IEEE Trans. Transport. Electrific*, vol. 5, no. 4, pp. 1040-1059, Dec. 2019.

[10] Y. Wang, M. Wang and D. Lin, "The duality of inductive power transfer and capacitive power transfer," 2020 8th *International Conference on Power Electronics Systems and Applications* (PESA), 2020, pp. 1-5.

[11] J. Sallan, J. L. Villa, A. Llombart and J. F. Sanz., "Optimal design of ICPT systems applied to electric vehicle battery charge," *IEEE Trans. Ind. Electron.*, vol. 56, no. 6, pp. 2140-2149, June 2009.

[12] L. Gu, G. Zulauf, A. Stein, P. A. Kyaw, *et al*., "6.78-MHz wireless power transfer with self-resonant coils at 95% dc–dc efficiency," *IEEE Trans. Power Electron*, vol. 36, no. 3, pp. 2456-2460, March 2021.

[13] Y. Zhang, Z. Yan, T. Kan, X. Zeng, S. Chen and C. C. Mi., "Modeling and analysis of a strongly coupled series–parallel-compensated wireless power transfer system," *IEEE J. Emerg. Sel. Topics Power. Electron*, vol. 7, no. 2, pp. 1364-1370, June 2019.

[14] A. Kuperman, "Additional two-capacitor basic compensation topologies for resonant inductive WPT links," *IEEE Trans. Power Delivery*, vol. 35, no. 5, pp. 2568-2570, Oct. 2020.

[15] Y. Liu, T. Wu and M. Fu, "Interleaved capacitive coupler for wireless power transfer," *IEEE Trans. Power Electron*, vol. 36, no. 12, pp. 13526-13535, Dec. 2021.

[16] T. Komaru and H. Akita, "Positional characteristics of capacitive power transfer as a resonance coupling system," *in Proc. IEEE Wireless Power Transf.*, 2013, pp. 218–221.

[17] Y. Wang, H. Zhang and F. Lu, "Capacitive power transfer with series-parallel compensation for step-up voltage output," *IEEE Trans. Ind. Electron*., vol. 69, no. 6, pp. 5604-5614, June 2022.

[18] Y. Wang, H. Zhang and F. Lu., "Current-Fed capacitive power transfer with parallel-series compensation for voltage step-down," *IEEE J. Emerg. Sel. Topics Ind. Electron*., vol. 3, no. 3, pp. 454-464, July 2022.

[19] S. Li and C. Mi, "Wireless power transfer for electric vehicle applications," *IEEE J. Emerging Sel. Top. Power Electon*., vol. 3, no. 1, pp. 4–17, Mar. 2015.

[20] H. J. Kim, H. Hirayama, S. Kim, *et al*., "Review of near-field wireless power and communication for biomedical applications," *IEEE Access*, vol. 5, pp. 21264-21285, Oct. 2017.

[21] S. Y.R. Hui, "Planar wireless charging technology for portable electronic products and Qi," *Proc. IEEE*, vol. 101, no. 6, pp. 1290–1301, Jun. 2013.

[22] M. Tamura, Y. Naka, K. Murai and T. Nakata, "Design of a capacitive wireless power transfer system for operation in fresh water," *IEEE Trans. Microw. Theory Tech*., vol. 66, no. 12, pp. 5873-5884, Dec. 2018

[23] D. C. Ludois, J. K. Reed and K. Hanson, "Capacitive power transfer for rotor field current in synchronous machines," *IEEE Trans. Power Electron*, vol. 27, no. 11, pp. 4638-4645, Nov. 2012.

[24] E. Culurciello and A. G. Andreou, "Capacitive inter-chip data and power transfer for 3-D VLSI," *IEEE Transactions on Circuits and Systems II*: *Express Briefs*, vol. 53, no. 12, pp. 1348-1352, Dec. 2006.

[25] Z. Hu, M. Goodall, L. Zhao, Q. Zhu and A. P. Hu, "A comparative study of different compensation topologies for capacitive power transfer," 2020 *IEEE PELS Workshop on Emerging Technologies: Wireless Power Transfer* (*WoW*), 2020, pp. 389-394.

[26] F. Lu, H. Zhang, et al., "A double-sided LCLC-compensated capacitive power transfer system for electric vehicle charging," *IEEE Trans. Power Electron*, vol. 30, no. 11, pp. 6011-6014, Nov. 2015.

[27] J. Xia, X. Yuan, S. Lu, J. Li, S. Luo and S. Li, "A two-stage parameter optimization method for capacitive power transfer systems," *IEEE Trans. Power Electron*., vol. 37, no. 1, pp. 1102-1117, Jan. 2022.

[28] H. Zhang, F. Lu, H. Hofmann, W. Liu, and C. Mi, "A four-plate compact capacitive coupler design and LCL-compensated topology for capacitive power transfer in electric vehicle charging application," *IEEE Trans. Power Electron*., vol. 31, no. 12, pp. 8541–8551, Dec. 2016.

[29] Y. Wang, *et. al*., "Review, analysis, and design of four basic CPT topologies and the application of high-order compensation networks," *IEEE Trans. Power Electron*, vol. 37, no. 5, pp. 6181-6193, May 2022.

[30] Y. Wang, J. Mai, *et al*., "Analysis and design of an IPT system based on S/SP compensation with improved output voltage regulation," *IEEE Trans. Ind. Informat*., vol. 16, no. 5, pp. 3256-3266, May 2020.

[31] Y. Wei and F. Wu, "Indirect control strategy of secondary current for LCC-Series compensated wireless power transfer system based on primary current closed-loop control," *IEEE Trans. Transport. Electrific*, vol. 8, no. 2, pp. 1553-1565, June 2022.

[32] Z. Yan, Y. Zhang, B. Song, K. Zhang, T. Kan, C. Mi, "An LCC-P compensated wireless power transfer system with a constant current output and reduced receiver size," *Energies*, 12(1):172, 2019.

[33] M. Xiong, *et al*, "Design of the LCC-SP topology with a current doubler for 11-kW wireless charging system of electric vehicles," *IEEE Trans. Transp. Electrific*., vol. 7, no. 4, pp. 2128-2142, Dec. 2021.

[34] A. Bilal, S. Kim, et al., "Analysis of IPT intermediate coupler system for vehicle charging over large air gaps," *IEEE J. Emerg. Sel. Topics Ind. Electron.*, vol. 3, no. 4, pp. 1149-1158, Oct. 2022.

[35] S. Li, W. Li, J. Deng, *et al*., "A double-sided LCC compensation network and its tuning method for wireless power transfer," *IEEE Trans. Veh. Technol*., vol. 64, no. 6, pp. 2261-2273, June 2015.

[36] Kurs A., Karalis A., *et al*. Wireless power transfer via strongly coupled magnetic resonances. *Science*, 2007, 317(5834): 83-86.

[37] A. Costanzo, M. Dionigi, F. Mmastri, *et al*., "Rigorous network modeling of magnetic-resonant wireless power transfer," *Wireless Power Transf*., vol. 1, no. 1, pp. 27–34, Apr. 2014.

[38] X. Wu, Y. Su, A. P. Hu, L. J. Zou and Z. Liu, "A sleeve-type capacitive power transfer system with different coupling arrangements for rotary application," *IEEE Access*, vol. 8, pp. 69148-69159, 2020.

Yao Wang (S'21) received his B.S. and M.S. degrees in electrical engineering from Northwestern Polytechnical University, Xi'an, China, in 2017 and 2020, respectively.

He is currently pursuing his Ph.D. degree in electrical engineering at Drexel University, Philadelphia, PA, United States. His research interest focuses on wireless power transfer technology and resonant converter.

Hua Zhang (S'14–M'17) received B.S., M.S. and Ph.D. degree in electrical engineering from Northwestern Polytechnical University, Xi'an, China, in 2011, 2014, and 2017, respectively.

She is now an assistant professor in Rowan University, NJ, USA starting from September 2022. Her research focuses on high voltage power conversion technology for electric vehicle and power grid applications.

Yue Cao (Senior Member, IEEE) received the B.S. degree (Hons.) in electrical engineering with a second major in mathematics from the University of Tennessee, Knoxville, TN, USA, in 2011, and the M.S. and Ph.D. degrees in electrical engineering from the University of Illinois at Urbana–Champaign (UIUC), Champaign, IL, USA, in 2013 and 2017, respectively.

Dr. Cao is currently an Assistant Professor with the Energy Systems Group at Oregon State University (OSU), Corvallis, OR, USA. Before joining OSU, he was a Research Scientist with the Propulsions Team at Amazon Prime Air in Seattle, WA, USA. He was a Power Electronics Engineer Intern with Special Projects Group at Apple Inc., Cupertino, CA, USA; Halliburton Company, Houston, TX, USA; and Oak Ridge National Laboratory, TN, USA. He was a Sundaram Seshu Fellow in 2016 at UIUC, where he was a James M. Henderson Fellow in 2012. His research interests include power electronics, motor drives, and energy storage with applications in renewable energy integration and transportation electrification.

Dr. Cao was a national finalist of the USA Mathematical Olympiad (USAMO) in 2006 and 2007. He received the Myron Zucker Student Award from the IEEE Industry Applications Society (IAS) in 2010. He won the Oregon State Learning Innovation Award for transformative education in 2020. He is a recipient of the 2022 NSF CAREER award. He is selected into U.S. National Academy of Engineering (NAE) Frontiers of Engineering (FOE) class of 2022. Dr. Cao was the Special Sessions Chair of the 2022 IEEE Energy Conversion Congress Expo (ECCE) and the Tutorials Chair of 2021 ECCE. He is a board member and Award Chair of IEEE Power Electronics Society (PELS) TC11 – Aerospace Power. In 2020, he helped establish an IEEE PELS Chapter at OSU. He is currently an Associate Editor for IEEE Transactions on Transportation Electrification and an Associate Editor for IEEE Transactions on Industry Applications.

Fei Lu (S'12–M'17) received the B.S. and M.S. degree from Harbin Institute of Technology, Harbin, China, in 2010 and 2012, respectively, and the Ph.D. degree from University of Michigan, Ann Arbor, Michigan, USA, in 2017, all in electrical engineering.

He is currently an assistant professor in the Department of Electrical and Computer Engineering in Drexel University, Philadelphia, PA, USA. His research topic focuses on power electronics and the application of electric vehicle charging.